Applied Surface Science 533 (2020) 147503

Contents lists available at ScienceDirect

Applied Surface Science

journal homepage: www.elsevier.com/locate/apsusc

DFT band alignment of polar and nonpolar GaN/$MgGeN_2$, ZnO/$MgGeN_2$ and GaN/ZnO heterostructures for optoelectronic device design

Chaiyawat Kaewmeechai[a], Yongyut Laosiritaworn[a,b], Atchara Punya Jaroenjittichai[a,b,*]

[a] Department of Physics and Materials Science, Faculty of Science, Chiang Mai University, 239 Huay Kaew Road, Muang Chiang Mai 50200, Thailand
[b] Research Center in Physics and Astronomy, Faculty of Science, Chiang Mai University, Chiang Mai 50200, Thailand

ARTICLE INFO

Keywords:
DFT
GaN
ZnO
$MgGeN_2$
Band alignment
Heterojunction

ABSTRACT

We calculated the band alignment among $MgGeN_2$, ZnO and GaN compounds using density functional theory (DFT) calculations. The norm-conserving pseudopotentials approach was performed to determine the band gap of each compound. The band offsets at the interfaces of GaN/$MgGeN_2$ and ZnO/$MgGeN_2$ were calculated from the differences in the bulk band edges including the interfacial dipole-potentials. Moreover, the effect of strain was also investigated to govern the lattice mismatches between $MgGeN_2$ and substrates (i.e. GaN and ZnO). We found that the band alignment of nonpolar heterojunctions is type-I for GaN/$MgGeN_2$ and type-II for ZnO/$MgGeN_2$ respectively. From these results, the band offsets of GaN/ZnO were extracted by using transitivity rule and confirmed with the direct calculation. Moreover, the polar band offsets shift from nonpolar ones and change the band alignment of ZnO/$MgGeN_2$ with (Mg,Ge)-O interface to type-I. These calculated band alignments present the potential of using $MgGeN_2$ in optoelectronic applications as an electron blocking layer for ZnO-based UV-LED and a quantum-well barrier for ZnO and GaN-based UV laser diode.

1. Introduction

The achievement of material growth in III-nitride semiconductors such as InN, GaN, and AlN in wurtzite structure enables numerous applications in modern electronics, especially high frequencies applications e.g. blue-green light-emitting diodes (LEDs), high-resolution printing, and optical data storage devices [1,2] and also power transistors for communication technology [3]. In commerce, LEDs based on III-N are manufactured as a double heterostructure (DH). It consists of three semiconductors as an n-type/intrinsic/p-type sandwich. Two semiconductors, n-type and p-type, are placed on two sides of the intrinsic semiconductor, which has a smaller band gap. The band alignment of all semiconductors in DH is type-I (straddling gap), which the larger gap semiconductors play a role as a wall of the quantum well to confine charges within a smaller band gap semiconductor. However, III-N is the binary compounds, which contain only one atom on cation site. This leads to lack of flexibility to modify electronic properties. Besides, Gallium (Ga) and Indium (In) are highly required for many technologies e.g. GaAs based-transistors; Indium tin oxide (ITO) in liquid-crystal displays (LCD), etc. Therefore, the ternary nitride semiconductors, II-IV-N_2, based on abundant elements have been proposed to be the alternative materials instead of III-N compounds [4,5]. It is expected that the property-trend of these orthorhombic II-IV-N_2 semiconductors should be similar to those of the wurtzite III-N compounds. $MgGeN_2$ is one of the attractive materials from these II-IV-N_2 series. It was predicted to have a lattice constant as a_w = 3.250 Å [5] and a wide-direct band gap as 5.14 eV [5] which are comparable to those of GaN (3.189 Å, 3.51 eV) and AlN (3.112 Å, 6.25 eV) [6]. It should be noted that, a_w is a lattice constant in wurtzite system which is equal to $b/2$, where b is a lattice constant in an orthorhombic system. Therefore, it is possible to grow $MgGeN_2$ with III-N to form the effective heterojunction for optoelectronics because they possess a small lattice mismatch of a few percent. Furthermore, ZnO also draws our attraction to build the heterostructure with $MgGeN_2$ due to its similar lattice constant and band gap to GaN. In addition, ZnO seems to be a good candidate for LED due to its excellent luminescent properties [7], but ZnO is still difficult to be doped as p-type semiconductor and to form a double quantum well heterostructure with GaN and AIN due to its type-II band alignment (staggered gap) [8,9]. In the past decade, to solve these problems, the p-GaN was used instead of p-ZnO. Nevertheless, the LEDs based on p-GaN/n-ZnO give a broad electroluminescence spectrum due to the emissions from both GaN and ZnO regions. To improve the electroluminescence, the electron blocking layer (EBL) such as MgO and AlN are placed at the interface of p-GaN/n-ZnO to block electrons moving to an n-ZnO region. Then, the strong emission intensity of n-ZnO can be achieved [10]. Moreover, by synthesis O-polar ZnO films on

* Corresponding author.
E-mail address: atcharapunya@gmail.com (A.P. Jaroenjittichai).

https://doi.org/10.1016/j.apsusc.2020.147503
Received 5 May 2020; Received in revised form 22 June 2020; Accepted 8 August 2020
Available online 12 August 2020
0169-4332/

N-polar GaN substrates, the stronger emission originating from ZnO in p-GaN/n-ZnO based LED was produced more than that from Zn-polar ZnO grown on Ga-polar GaN substrates [11]. It implies that the atomic interfacial structures are crucial for designing optoelectronic devices. These characteristics of the interface will directly affect the band alignment or the energy band offsets among semiconductors. However, the study of band alignment between $MgGeN_2$ and ZnO or $MgGeN_2$ and GaN has recently found in only one paper [12] unlike the band offset between ZnO and GaN [9,12–19].

Therefore, we investigated the band alignment among $MgGeN_2$, ZnO and GaN based on DFT-HSE. The electrostatic potential across heterojunctions among these materials and the dipole potentials at their interfaces were extracted in both nonpolar and polar directions by using three-step approach. For polar direction, two possible interfaces of heterojunctions were studied separately by vacuum inserting technique. At last, the variation of band offsets including and excluding strain effects in different interfacial orientations were clarified.

2. Computational details

The calculation in this work was performed using DFT based on norm-conserving pseudopotentials with plane wave basis sets [20]. All relaxed structures of bulk materials were obtained using the local density approximation (LDA). The plane wave cutoff energy was defined as 80 Ry with k-point mesh of 4 × 4 × 4. For the band gap calculation, we included hybrid functional from Heyd-Scuseria-Ernzerhof (HSE) approach [21] with optimized norm-conserving Vanderbilt pseudopotentials [22]. The mixing parameter, α, which represents the fraction between short-range part of nonlocal Hartree-Fock and generalized gradient approximation (GGA) exchanges, were defined as 0.31 and 0.38 for GaN and ZnO respectively [13,23], while for $MgGeN_2$, it was defined as α = 0.25 to give a consistent band gap to QSGW results [12,24]. Then, the strained valence band offsets (VBO) of heterojunction between semiconductors *A* and *B*, $VBO(A/B)$, was performed by using Eq. (1) and the effect of deformation potential, ΔE_{DP}, is corrected to obtained the natural band offsets or the unstrained valence band offsets, $VBO^{nat}(A/B)$, as followed in Eq. (2). Then, the accompanied conduction band offsets (CBO) can be gained by adding the difference between band gaps of A and B. Note that, for the symbol of A/B heterojunction, the left-hand side (A) is the substrate and the right-hand side (B) is the material grown on top of the substrate.

$$\begin{aligned} VBO(A/B) &= \Delta E_b^B - \Delta E_b^A + \Delta V_D \\ &= (E_v^B - \bar{\bar{V}}_B) - (E_v^A - \bar{\bar{V}}_A) + (\bar{\bar{V}}_A - \bar{\bar{V}}_B) \end{aligned} \quad (1)$$

$$VBO^{nat}(A/B) = VBO(A/B) + \Delta E_{DP} \quad (2)$$

The first and second terms on the right-hand side of Eq. (1); ΔE_b^B and ΔE_b^A denote the bulk band edges of semiconductors *A* and *B*. The bulk band edge is the difference between the valence band maximum (E_v) and the reference energy level ($\bar{\bar{V}}$) which is a macroscopic-averaged electrostatic potential (MAEP) of a bulk material. The third term (ΔV_D) is a dipole potential or the difference between the MAEP of *A* and *B*, obtaining from A/B-supercell-calculation [25]. Moreover, $\bar{\bar{V}}$ is also denoted as a volume-averaged electrostatic potential (VAEP) or an average of planar-averaged electrostatic potential (PAEP), which can be obtained from $\bar{\bar{V}}(z) = \frac{1}{L}\int_{-L/2}^{L/2} \bar{V}(z')dz'$, where, $\bar{V}$ is a PAEP, $\bar{V}(z) = \frac{1}{S}\int_S V(x, y, z)dxdy$, *L* is a distance between atomic layers and *S* is the area which is parallel to the interface. The MAEP is commonly used as the referent energy for band offsets calculation similar to a core level in XPS-like approach [25]. The last term in Eq. (2) is the reference energy level shift due to the deformation potential induced by strain. In short, it is called as a deformation potential energy(ΔE_{DP}). Thus $\Delta E_{DP} = \Delta E_{[100]} + \Delta E_{[001]}$ and $\Delta E_{DP} = \Delta E_{[100]} + \Delta E_{[010]}$ for nonpolar and polar heterostructures respectively. We note that the lattice parameters in wurtzite can be convert to orthorhombic parameters using the following relations $a = \sqrt{3}a_w$, $b = 2a_w$ and $c = c_w$ as shown in Fig. 1. The nonpolar directions for wurtzite and orthorhombic are $[10\bar{1}0]$ and $[0\,1\,0]$ while the polar directions are $[0\,0\,0\,1]$ and $[0\,0\,1]$ respectively.

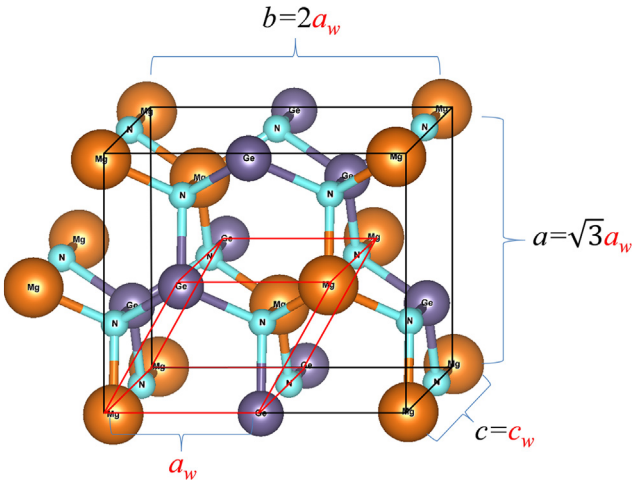

Fig. 1. The overlaid wurtzite unit cell (red) on an orthorhombic unit cell (black). The relations between wurtzite and orthorhombic lattice parameters are; $a = \sqrt{3}a_w$; $b = 2a_w$; and $c = c_w$. (For interpretation of the references to colour in this figure legend, the reader is referred to the web version of this article.)

Here, we assumed that GaN and ZnO were the substrates with fixed lattice parameters, while $MgGeN_2$ was grown on top with the same in-plane lattice constants as those of substrates. The out-of-plain lattice constant of $MgGeN_2$ was defined as that of its bulk. Thus, only ΔE_{DP} of $MgGeN_2$ is considered in calculation of unstrained band offsets. To model the growing of $MgGeN_2$ on ZnO or GaN with strained condition, we created the supercell heterojunction of 6 unit-cells, containing 96 atoms as presented in Fig. 2. The ΔE_{DP} was calculated by using the three-step approach [26]. For supercell calculation, we employed the cut-off plane-wave energy as 80 Ry and the k-point grid along interface direction was reduced to 1 while the other directions were kept as 4.

In particular, for the polar heterojunction with growth direction $[0\,0\,1]$, different interfaces appear due to the periodic boundary condition. To study one single interface separately, the vacuum inserting will be performed to handle the induced filed from an undesired interface. However, there is an artificial electric field across the vacuum region, which can be compensated by the dipole correction. This correction was proposed as $V_{dip}(z) = 4\pi m\left(\frac{z}{z_m} - \frac{1}{2}\right)$, $0 < z < z_m$ [27] where, *m* is the surface dipole density obtained from $m = \int_{-\infty}^{\infty} \rho_{av}(z')z'dz'$ and z_m is the length of supercell. The size of a vacuum region is $z_m/2$. This compensation makes the flat MAEP of ideal vacuum region occur. The interfaces in polar heterojucntions were named after the interfacial atomic structure or atoms at the interface. As shown in Fig. 2, there are two possible (Mg,Ge)-N and Ga-N interfaces for GaN/$MgGeN_2$, (Mg,Ge)-O and Zn-N interfaces for ZnO/$MgGeN_2$, and Zn-N and Ga-O interface for GaN/ZnO.

3. Results and discussions

3.1. Crystal structures, band gaps, and deformation potential energies

The lattice parameters of $MgGeN_2$, GaN, and ZnO obtained from LDA are in good agreement with previous calculations using the same method [5,23,28] but are slightly less than experimental values as expected [29–31]. The lattice parameters and the lattice mismatches of $MgGeN_2$ respect to GaN and ZnO are listed in Table 1. It shows the small lattice mismatches within 3% in all directions, which means high possibility to grow heterojunction among these compounds. After the crystal structure optimization, we performed the calculations of HSE-

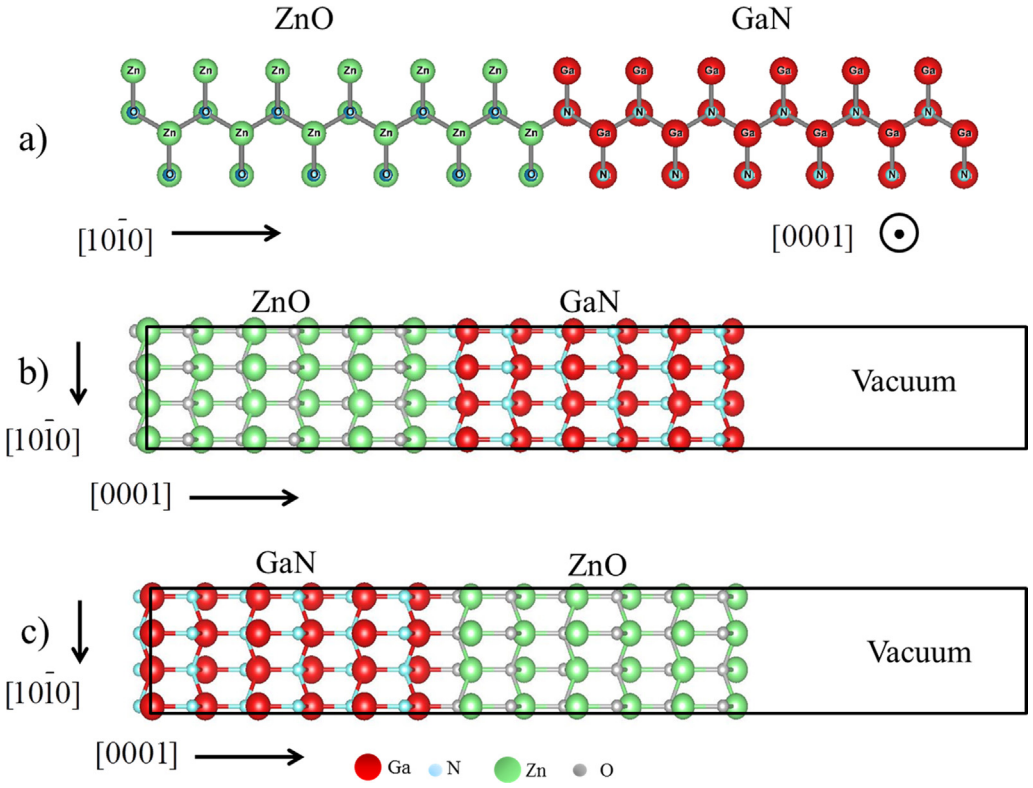

Fig. 2. shows supercell of (a) nonpolar and polar GaN/ZnO heterojunctions where (b) Zn and N atoms are located at the interface, named as Zn-N interface, (c) Ga and O atoms are located at the interface, called as Ga-O interface.

band gap both with and without *d*-electrons as valence electrons in optimized Vanderbilt norm-conserving approach. It shows that all these materials have direct band gaps and performing without *d*-orbital valence electrons in ZnO and GaN requires high mixing parameters (α) to obtain gaps close to the reliably experimental values. Thus, we included *d*-orbitals as valence bands of Ga, Zn and Ge atoms. The band gaps and bulk band edges obtained from HSE are also listed in Table 1. By using α as 0.31 for GaN and α as 0.38 for ZnO [13]. Our calculated band gaps of GaN (3.46 eV) and ZnO (3.49 eV) are consistent to previous photoluminescence spectral measurement for GaN (3.47 eV) [6] and ZnO (3.44 eV) [32] respectively. For $MgGeN_2$, we performed HSE calculation with α = 0.25 and got band gap as 4.52 eV. This is close to the recently calculated band gap of $MgGeN_2$ using the QSGW method which are 4.11 eV [24] and 4.71 eV [12] respectively. It is noticeable that the band gap of $MgGeN_2$ was significantly reduced from 5.14 eV of the first QSGW work due to the lack of 3*d*-Ge semicore states in its calculation [5]. Recently, $MgGeN_2$ was synthesized by the ammonothermal method and has the optical band gap of 3.2 eV measured from the diffuse reflectance spectra [33]. However, the accurate measurement of $MgGeN_2$-band gap is remaining to be clarified because there are a few works reported recently.

To obtain the deformation potential energies (ΔE_{DP}), three different A/B heterojunctions were modeled i.e. GaN/$MgGeN_2$, ZnO/$MgGeN_2$, and GaN/ZnO, where A is a substrate and B is a strained compound. The

Table 2
Deformation potential energy (ΔE_{DP}) in each direction and total ΔE_{DP} of $MgGeN_2$ and ZnO in eV, note that only two in-plane-ΔE_{DP} occur in a both polar and nonpolar supercell.

Compounds	Type of supercell	ΔE_{DP} in each direction			Total
		[100]	[010]	[001]	ΔE_{DP}
$MgGeN_2$ (GaN-substrate)	nonpolar	0.19	–	0.16	0.30
	polar	0.19	−0.41	–	−0.22
$MgGeN_2$ (ZnO-substrate)	nonpolar	0.18	–	0.13	0.31
	polar	0.18	−0.22	–	−0.03
ZnO (GaN-substrate)	nonpolar	−0.07	–	0.02	−0.05
	polar	−0.07	−0.08	–	−0.15

ΔE_{DP} due to transformation from unstrained B to strained B, was acquired from the homojunction-supercell-calculation following the three-step method [26] and shown in Table 2. It shows that ΔE_{DP} in each direction of $MgGeN_2$ increases with the rise of the lattice mismatches between $MgGeN_2$ and substrates. However, ΔE_{DP} of strained $MgGeN_2$ on top of GaN and ZnO substrates are slightly different, especially in nonpolar supercell. This is because the lattice mismatch

Table 1
Lattice parameters, lattice mismatches, HSE band gaps (E_g) and bulk band edges (ΔE_b) of $MgGeN_2$, GaN, and ZnO.

Compounds	Lattice parameters (Å)			Lattice mismatches (%)			E_g (eV)	ΔE_b (eV)
	a	*b*	*c*	*a*	*b*	*c*		
$MgGeN_2$	5.39	6.50	5.07	–	–	–	4.52	3.88
ZnO	5.51	6.36	5.14	−2.18	2.20	−1.36	3.46	1.90
GaN	5.47	6.32	5.15	−1.46	2.85	−1.55	3.49	4.06

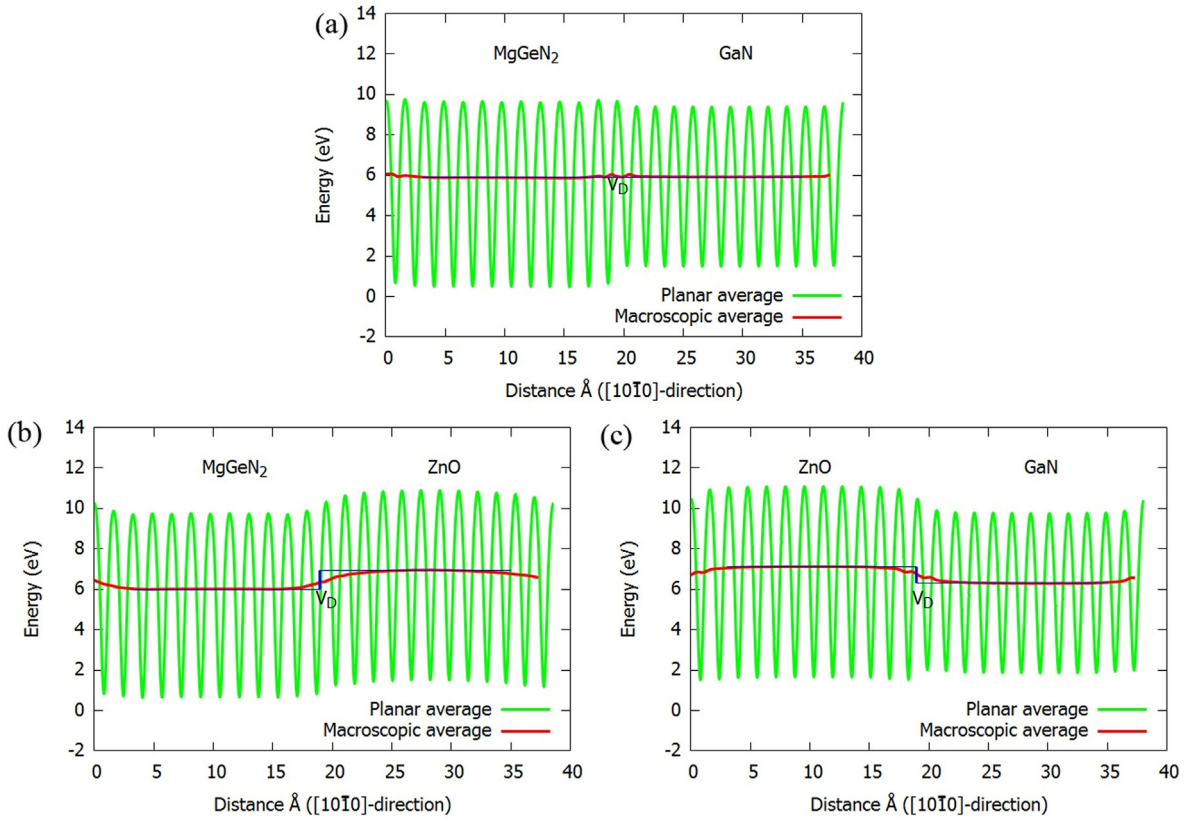

Fig. 3. Averaged electrostatic potentials of nonpolar (a) GaN/$MgGeN_2$, (b) ZnO/$MgGeN_2$ and (c) GaN/ZnO heterojunction.

between GaN and ZnO are less than 1%. This is also true when the smallΔE_{DP} of strained GaN on top of ZnO was directly calculated as shown in Table 2.

3.2. Band offsets of nonpolar heterojunctions

For nonpolar heterojunctions, the flat MAEP can be observed in the region far away from interface as shown in Fig. 3 (a–c). This denotes the zero-electric field in a bulk structure and can represent the bulk-like region of each semiconductor. The magnitude of potential difference at the interfaces represents the ΔV_D, which are listed in Table 3 for all interfaces. From Table 3, ΔV_D at GaN/$MgGeN_2$ interface is almost zero. This suggests the small potential difference in nitride/nitride heterojunction as seen in Fig. 3(a). Otherwise, at oxide/nitride interfaces, i.e. ZnO/$MgGeN_2$ and GaN/ZnO interfaces, a large interface dipole is generated as seen in Fig. 3(b) and (c). Later, nonpolar band offsets of heterojunctions were calculated as shown in Table 3. The strained band offsets of GaN/$MgGeN_2$ and ZnO/$MgGeN_2$ heterojunctions are 0.21 and −1.04 eV for valence bands, and −0.82 and −2.10 eV for conduction bands. Thus, the band alignment of GaN/$MgGeN_2$ and ZnO/$MgGeN_2$ are clarified in type-I and type-II respectively. For unstrained band offsets, which including ΔE_{DP}, VBO and CBO are shifted to 0.56 and −0.47 eV for GaN/$MgGeN_2$ and −0.73 and −1.79 eV for ZnO/$MgGeN_2$ as shown in Table. 3. Thus, the band alignment of GaN/$MgGeN_2$ and ZnO/$MgGeN_2$ are still clarified in type-I and type-II respectively. These types of band alignment are in agreement with previous work using the electron affinity rule, although the smaller VBO of 0.32 and −0.01 eV for GaN/$MgGeN_2$ and ZnO/$MgGeN_2$ were reported [12]. Note that, the electron affinity rule is the simplest model for VBO, it does not included the interfacial dipole formation and strain effects.

Table 3
Dipole potential, valence and conduction band offsets of nonpolar heterojunctions in eV.

A/B heterojunction	ΔV_D	Strained*		Unstrained**	
		VBO	*CBO*	VBO^{nat}	CBO^{nat}
GaN/$MgGeN_2$	0.03	0.21	−0.82	0.56	−0.47
ZnO/$MgGeN_2$	0.93	−1.04	−2.10	−0.73	−1.79
GaN/ZnO (Transitivity)	–	–	–	1.29	1.32
GaN/ZnO (Direct cal.)	−0.83	1.32	1.36	1.27	1.30

* "Strained" implies that material B is under strain.

** "Unstrained" means that band offsets are corrected by adding ΔE_{DP} or the natural band offsets.

Moreover, by applying the transitivity rule to the unstrained band offsets of GaN/$MgGeN_2$ and ZnO/$MgGeN_2$, the band offsets between GaN and ZnO were obtained as 1.29 and 1.32 eV for VBO and CBO respectively. These results are well-compared with the direct calculations of unstrained GaN/ZnO from this work, which are 1.27 and 1.30 eV for VBO and CBO respectively. The agreement of these offsets obtained from transitivity rule and direct calculation supports that our band-offset calculation is reliable. In addition, the VBO of nonpolar GaN/ZnO in this work are also well-compared with previous PBE-HSE calculation with projected augmented wave (PAW) methods. Their VBO of GaN/ZnO are 1.59 eV [14] and 1.31 eV [13].

3.3. Band offsets of polar heterojunctions

As the same as nonpolar heterojunction, the supercell was modeled to extract theΔV_D at the interface. Generally, wurtzite semiconductors exhibit a non-vanish dipole in [0 0 0 1] direction due to lack of inversion symmetry. This induces an internal electric field and causes inclined MAEP inside materials. The PAEP and MAEP of GaN/$MgGeN_2$, ZnO/$MgGeN_2$ and GaN/ZnO heterojunctions are plotted as shown in Fig. 4(a-f). For GaN/$MgGeN_2$ heterojunction, as seen in Fig. 4(a) and (b), two different interfacial atomic structures, Ga-N and (Mg,Ge)-N interfaces,

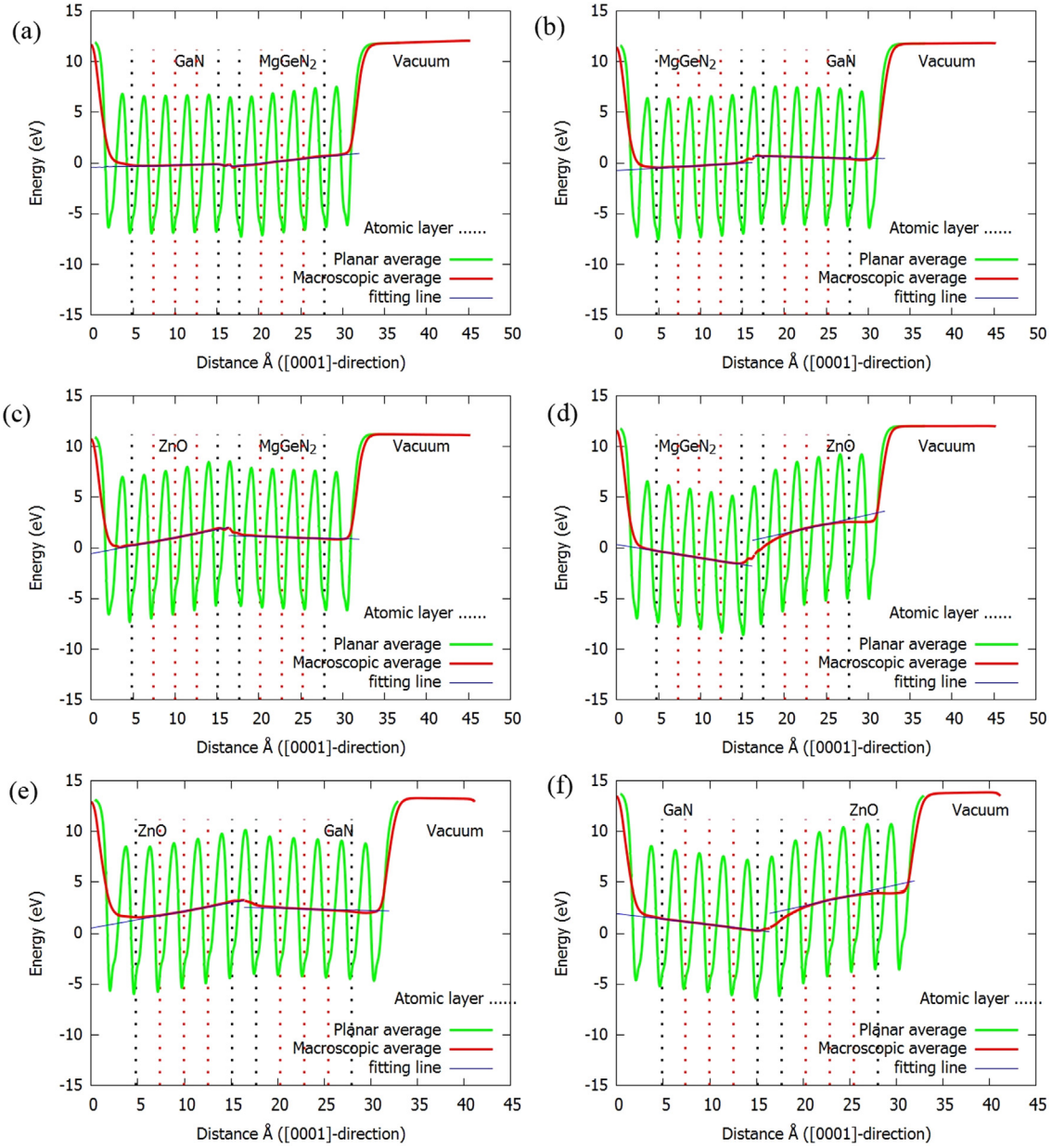

Fig. 4. Averaged electrostatic potentials of polar heterojunctions. (a) GaN/$MgGeN_2$ with Ga-N interface, (b) GaN/$MgGeN_2$ with (Mg,Ge)-N interface, (c) GaN/$MgGeN_2$ with Zn-N interface, (d) ZnO/$MgGeN_2$ with (Mg,Ge)-O interface, (e) GaN/ZnO with Zn-N interface, and (f) GaN/ZnO with Ga-O interface.

Table 4
Dipole potential energy, (ΔV_D), valence band offset (*VBO*), and conduction band offset (*CBO*) of polar heterojunction in eV.

Heterojunctions	Interfacial atomic structures	ΔV_D	Strained		Unstrained	
			VBO	*CBO*	VBO^{nat}	CBO^{nat}
GaN/$MgGeN_2$	(Mg,Ge)-N	0.68	0.86	−0.17	0.65	−0.38
	Ga-N	−0.11	0.29	−0.74	0.08	−0.95
ZnO/$MgGeN_2$	(Mg,Ge)-O	2.61	0.64	−0.42	0.61	−0.45
	Zn-N	−0.63	−1.34	−2.41	−1.37	−2.44
GaN/ZnO	Ga-O	1.93	0.22	0.26	0.07	0.11
	Zn-N	0.50	1.65	1.68	1.50	1.53

were modeled. In the same way, the Zn-N and (Mg,Ge)-O interfaces of ZnO/$MgGeN_2$ as well as Zn-N and Ga-O interfaces of GaN/ZnO were imitated as presented in Fig. 4(c-f). We assume that the effect of the interfacial dipole exists only in the two atomic layers near the interface. Thus, we firstly applied a linear least squares fitting, drawn as a blue lines in Fig. 4(a-f), to the MAEP of the middle three atomic layers which indicated by red dashed line. Next, ΔV_D, listed in Table 4, were obtained from the difference between two points which defined as the intersections of the blue fitting line and the interfacial atomic layer, indicated by a black dashed line in Fig. 4(a-f). The large ΔV_D occur at the (Mg,Ge)-O and Ga-O interfaces due to the strong internal electric field (steep MAEP-slope) inside materials. Finally, the band offsets in polar direction were calculated as presented in Table 4.

Strained and unstrained band offsets of polar heterojunctions are different from those of nonpolar ones due to the variation of energy shifts in ΔV_D andΔE_{DP}. Moreover, they also depend on their interfacial atomic structures as presented in Table 5. For GaN/$MgGeN_2$, the band alignments are classified in type-I, which is as same as that of nonpolar case. For ZnO/$MgGeN_2$, strained band offsets at Zn-N interface slightly differ from those without strain due to cancellation between compressed and extended lattices or owing smallΔE_{DP}. The band alignment

Table 5
Atomic electronegativity (χ), and electronegativity difference ($|\Delta\chi|$) for each interfacial atomic structures.

Atom	Electronegativity(χ) [34,35]	Interfacial atomic structures	Electronegativity difference ($|\Delta\chi|$)
Zn	1.59	(Mg,Ge)-N	1.42
O	3.61	Ga-N	1.31
N	3.07	(Mg,Ge)-O	1.97
Mg	1.29	Zn-N	1.48
Ge	1.99	Ga-O	1.85
Ga	1.76		
(Mg,Ge)*	1.64		

* Note that, for (Mg,Ge), $\chi$is the average between χ_{Mg} andχ_{Ge}.

at Zn-N interface is type-I but it turns to type-II for (Mg,Ge)-O interface. The dramatically large ΔV_Dat (Mg,Ge)-O interface is the reason for this change. The strength of interfacial dipole can be considered roughly from the difference between electronegativity (χ) of atoms at the interfaces. As seen in Table 5, χ of oxygen is the largest and electronegativity-difference ($|\Delta\chi|$) between (Mg,Ge) and O are the largest too. The band line-up of unstrained band offsets between any pair from $MgGeN_2$, ZnO and GaN is depicted in Fig. 5.

The band offsets of well-known polar GaN/ZnO heterojunction were also calculated in this work. For Zn-N interface, the unstrained VBO and CBO are large as 1.50 and 1.53 eV respectively. Conversely, For Ga-O interface, the unstrained VBO and CBO are very small as 0.07 and 0.11 eV respectively. This vast variation of band offsets could be explained from ΔV_D or $|\Delta\chi|$ like what occurs at (Mg,Ge)-O interface of $ZnO/MgGeN_2$ heterojunction. The dipole at Ga-O interface is much larger than that of Zn-N interface and this also can be explain from the trend of electronegativity. However, the band offsets of GaN/ZnO are found in type-II alignment for all interfacial atomic structures.

For our polar GaN/ZnO, the average of natural VBO is 0.78 eV which is comparable with 0.8 eV measured by X-ray photoelectron spectroscopy (XPS) [15] and 0.7 ± 0.1 eV measured by synchrotron radiation photoemission spectroscopy [16]. Nevertheless, there are various experimental and theoretical studies for band offsets of polar GaN/ZnO, but the results are still inconsistency. For example, VBO were reported as 1.37 eV by transitivity rule [9], 0.38 and 0.47 eV from two samples with XPS [17], 1.0 eV and 0.5 eV from cation and anion compensated PBE-DFT [18], and 1.6 eV by the repeated slab geometry with virtual-hydrogen-terminated surfaces [19].

3.4. Band offset and applications

From our calculated band offsets, we propose to use $MgGeN_2$ as electron blocking layer (EBL) in LED based on p-GaN/n-ZnO for enhancing the emission in ZnO. A thin film of $MgGeN_2$ with large CBO should be placed between GaN and ZnO to form p-GaN/$MgGeN_2$/n-ZnO heterojunctions as depicted in Fig. 6(a). This should be noted that the large CBO was found in nonpolar and Zn-N polar $ZnO/MgGeN_2$ heterojunctions. Under forward bias, the large CBO will block electrons that move from n-ZnO but holes can transfer from p-GaN to n-ZnO due to small VBO. Thus electrons and holes will have a chance to recombination in ZnO region. This could improve the efficiency of ZnO-based UV-LED.

Moreover, we suggest that $MgGeN_2$ and GaN have a potential to build a quantum well for UV-laser diode. This is because $GaN/MgGeN_2$ has a type-I alignment in both nonpolar and polar directions with large VBO and CBO. Then, $MgGeN_2/GaN/MgGeN_2$ could be created as a double heterostructure which can trap charge carriers in GaN region as seen in Fig. 6(b). $MgGeN_2$ can be also applied along InN semiconductors because, by considering the transitivity rule of $InN/GaN/MgGeN_2$ and using band gap of InN as 0.78 eV [6], the band alignment of $InN/MgGeN_2$ is also type-I. Similarly, $ZnO/MgGeN_2$ with (Mg,Ge)-O interface also shows the potential to construct a double heterojunction, $MgGeN_2/ZnO/MgGeN_2$, as shown in Fig. 6(c).

4. Conclusions

We presented the equilibrium crystal structures of $MgGeN_2$, GaN,

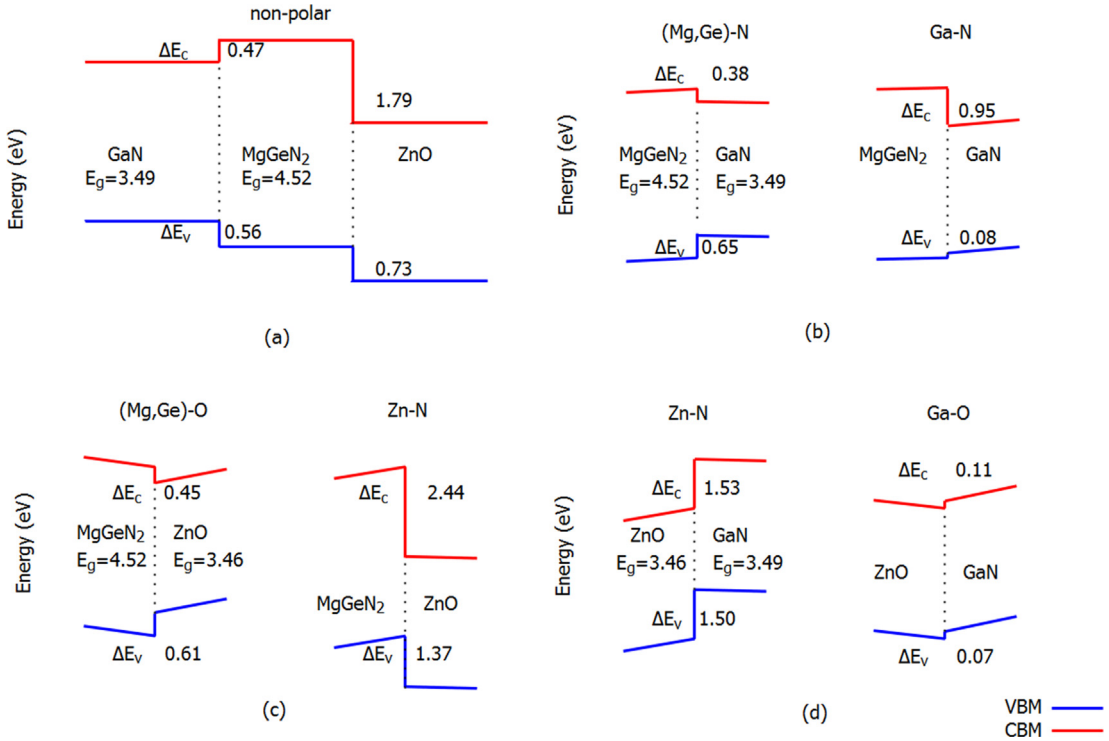

Fig. 5. The natural band alignment in (a) nonpolar $ZnO/MgGeN_2$ and $GaN/MgGeN_2$ heterojunctions, (b) polar $GaN/MgGeN_2$ heterojunction, (c) polar $ZnO/MgGeN_2$ heterojunction and (d) polar GaN/ZnO heterojunctions.

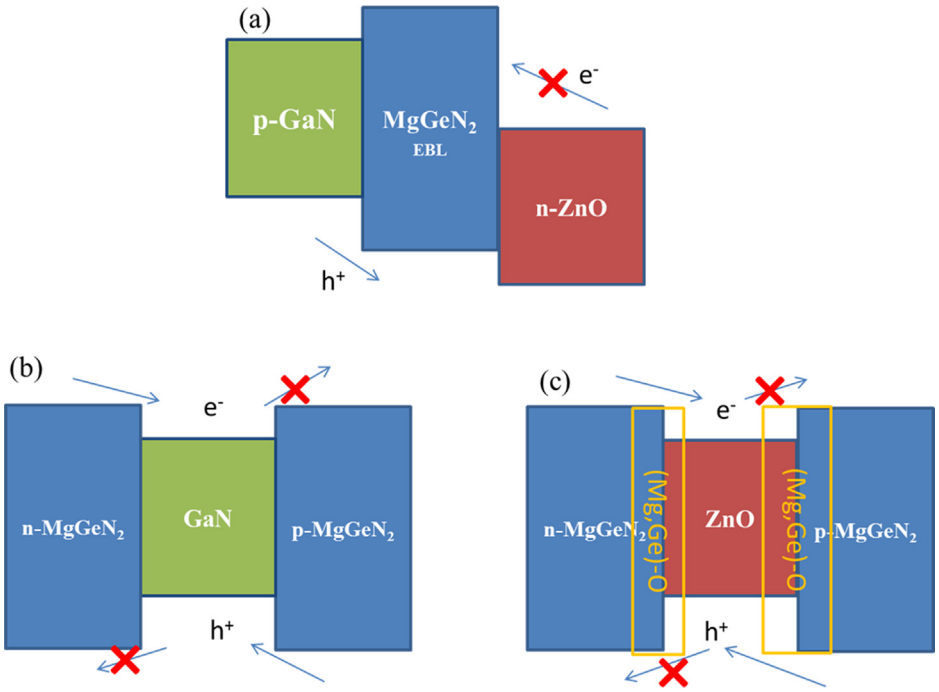

Fig. 6. Suggested application of heterostructures among $MgGeN_2$, ZnO and GaN. (a) $MgGeN_2$ as electron blocking layer in p-GaN/$MgGeN_2$/n-ZnO for UV-LEDs based on ZnO active layer (b) a double heterostructure of n-$MgGeN_2$/GaN/p-$MgGeN_2$ for UV-laser diode based on GaN-active layer, and (c) a double heterostructure of n-$MgGeN_2$/ZnO/p-$MgGeN_2$, with (Mg,Ge)-O interface, for UV-laser diode based on ZnO active layer.

ZnO by performing DFT. The lattice mismatches among these compounds were found within 3%, which shows their potential on heterostructure-construction. In addition, the HSE electronic structures reveal that all three semiconductors exhibits the direct band gaps which are well-compared with previous works. The energy gaps are 4.52, 3.49 and 3.46 eV for $MgGeN_2$, GaN and ZnO respectively. By considering the electrostatic potential with interfacial dipole and deformation potential energy, the natural band alignment of nonpolar GaN/$MgGeN_2$, ZnO/$MgGeN_2$ and GaN/ZnO were found in type-I, type II and type-II with the VBO of 0.56, −0.73 and 1.27 eV respectively. For polar heterojunctions, the interfaces containing oxygen, i.e. (Mg,Ge)-O and Ga-O interfaces in ZnO/$MgGeN_2$ and GaN/ZnO, show dramatically shift in band offsets due to the large electronegativity-difference. This changes the band alignment of ZnO/$MgGeN_2$, with (Mg,Ge)-O interface, from type- II to I while the other heterojunctions still have the same type with changed offsets. From the band offset calculation, we suggested that $MgGeN_2$ can be used as an electron blocking layer in ZnO-based UV LED especially by growing nonpolar or (Mg,Ge)-N polar ZnO/$MgGeN_2$. Furthermore, we also proposed the double heterostructure of n-$MgGeN_2$/GaN/p-$MgGeN_2$ for UV-laser diode based on GaN-active layer and n-$MgGeN_2$/ZnO/p-$MgGeN_2$, with (Mg,Ge)-O interface, for UV-laser diode based on ZnO active layer.

CRediT authorship contribution statement

Chaiyawat Kaewmeechai: Data curation, Methodology, Writing - original draft. **Yongyut Laosiritaworn:** Resources, Writing - review & editing. **Atchara Punya Jaroenjittichai:** Conceptualization, Investigation, Writing - review & editing.

Declaration of Competing Interest

The authors declare that they have no known competing financial interests or personal relationships that could have appeared to influence the work reported in this paper.

Acknowledgement

This work was supported by Thailand Research Fund under grant no. MRG6080237 and Chiang Mai University.

References

[1] F.A. Ponce, D.P. Bour, Nitride-based semiconductors for blue and green light-emitting devices, Nature 386 (1997) 351–359.
[2] J. Heber, Nobel Prize 2014: Akasaki, Amano & Nakamura, Nat. Phys. 10 (2014) 791.
[3] U.K. Mishra, L. Shen, T.E. Kazior, Y.-F. Wu, GaN-based RF power devices and amplifiers, Proc. IEEE 96 (2008) 287–305.
[4] A. Punya, W.R.L. Lambrecht, M. van Schilfgaarde, Quasiparticle band structure of Zn-IV-N_2 compounds, Phys. Rev. B 84 (2011) 165204.
[5] A.P. Jaroenjittichai, W.R.L. Lambrecht, Electronic band structure of Mg-IV-N_2 compounds in the quasiparticle-self-consistent GW approximation, Phys. Rev. B 94 (2016) 125201.
[6] I. Vurgaftman, J.R. Meyer, Band parameters for nitrogen-containing semiconductors, J. Appl. Phys. 94 (2003) 3675–3696.
[7] U. Ozgur, D. Hofstetter, H. Morkoc, ZnO devices and applications: a review of current status and future prospects, Proc. IEEE 98 (2010) 1255–1268.
[8] A. Janotti, C.G. Van de Walle, Fundamentals of zinc oxide as a semiconductor, Rep. Prog. Phys. 72 (2009) 126501.
[9] T.D. Veal, P.D.C. King, S.A. Hatfield, L.R. Bailey, C.F. McConville, B. Martel, J.C. Moreno, E. Frayssinet, F. Semond, J. Zúñiga-Pérez, Valence band offset of the ZnO/AlN heterojunction determined by x-ray photoemission spectroscopy, Appl. Phys. Lett. 93 (2008) 202108–202120.
[10] J.B. You, X.W. Zhang, S.G. Zhang, J.X. Wang, Z.G. Yin, H.R. Tan, W.J. Zhang, P.K. Chu, B. Cui, A.M. Wowchak, A.M. Dabiran, P.P. Chow, Improved electroluminescence from n-ZnO/AlN/p-GaN heterojunction light-emitting diodes, Appl. Phys. Lett. 96 (2010) 201102.
[11] J. Jiang, Y. Zhang, C. Chi, Z. Shi, L. Yan, P. Li, B. Zhang, G. Du, Improved ultraviolet emission performance from polarization-engineered n-ZnO/p-GaN heterojunction diode, Appl. Phys. Lett. 108 (2016) 063505.
[12] S. Lyu, W.R.L. Lambrecht, Band alignment of III-N, ZnO and II–IV-N_2 semiconductors from the electron affinity rule, J. Phys. D Appl. Phys. 53 (2019) 015111.
[13] T. Wang, C. Ni, A. Janotti, Band alignment and p-type doping of $ZnSnN_2$, Phys. Rev. B 95 (2017) 205205.
[14] Z. Wang, M. Zhao, X. Wang, Y. Xi, X. He, X. Liu, S. Yan, Hybrid density functional study of band alignment in ZnO–GaN and ZnO–$(Ga_{1-x}Zn_x)(N_{1-x}O_x)$–GaN heterostructures, Phys. Chem. Chem. Phys. 14 (2012) 15693–15698.
[15] S.-K. Hong, T. Hanada, H. Makino, Y. Chen, H.-J. Ko, T. Yao, A. Tanaka, H. Sasaki, S. Sato, Band alignment at a ZnO/GaN (0001) heterointerface, Appl. Phys. Lett. 78 (2001) 3349–3351.
[16] J.W. Liu, A. Kobayashi, S. Toyoda, H. Kamada, A. Kikuchi, J. Ohta, H. Fujioka, H. Kumigashira, M. Oshima, Band offsets of polar and nonpolar GaN/ZnO heterostructures determined by synchrotron radiation photoemission spectroscopy, Phys. Status Solidi B 248 (2011) 956–959.
[17] H.F. Liu, G.X. Hu, H. Gong, K.Y. Zang, S.J. Chua, Effects of oxygen on low-temperature growth and band alignment of ZnO/GaN heterostructures, J. Vac. Sci. Technol., A 26 (2008) 1462–1468.
[18] J. Von Pezold, P.D. Bristowe, Atomic structure and electronic properties of the

GaN/ZnO (0001) interface, J. Mater. Sci. 40 (2005) 3051–3057.
[19] T. Nakayama, M. Murayama, Electronic structures of hexagonal ZnO/GaN interfaces, J. Cryst. Growth 214–215 (2000) 299–303.
[20] M. Fuchs, M. Scheffler, Ab initio pseudopotentials for electronic structure calculations of poly-atomic systems using density-functional theory, Comput. Phys. Commun. 119 (1999) 67–98.
[21] J. Heyd, G.E. Scuseria, Efficient hybrid density functional calculations in solids: assessment of the Heyd–Scuseria–Ernzerhof screened Coulomb hybrid functional, J. Chem. Phys. 121 (2004) 1187–1192.
[22] D.R. Hamann, Optimized norm-conserving Vanderbilt pseudopotentials, Phys. Rev. B 88 (2013) 085117.
[23] C. Kaewmeechai, Y. Laosiritaworn, A.P. Jaroenjittichai, HSE hybrid functional calculation of band gap deformation potential in $MgGeN_2$, J. Phys. Conf. Ser. 1144 (2018) 012045.
[24] S. Lyu, W.R.L. Lambrecht, Quasiparticle self-consistent GW band structures of Mg-IV-N_2 compounds: The role of semicore d states, Solid State Commun. 299 (2019) 113664.
[25] L. Colombo, R. Resta, S. Baroni, Valence-band offsets at strained Si/Ge interfaces, Phys. Rev. B 44 (1991) 5572–5579.
[26] L. Lang, Y.-Y. Zhang, P. Xu, S. Chen, H.J. Xiang, X.G. Gong, Three-step approach for computing band offsets and its application to inorganic ABX_3 halide perovskites, Phys. Rev. B 92 (2015) 075102.
[27] L. Bengtsson, Dipole correction for surface supercell calculations, Phys. Rev. B 59 (1999) 12301.
[28] V. Srikant, D.R. Clarke, On the optical band gap of zinc oxide, J. Appl. Phys. 83 (1998) 5447–5451.
[29] H. Karzel, W. Potzel, M. Köfferlein, W. Schiessl, M. Steiner, U. Hiller, G.M. Kalvius, D.W. Mitchell, T.P. Das, P. Blaha, K. Schwarz, M.P. Pasternak, Lattice dynamics and hyperfine interactions in ZnO and ZnSe at high external pressures, Phys. Rev. B 53 (1996) 11425–11438.
[30] V. Darakchieva, B. Monemar, A. Usui, On the lattice parameters of GaN, Appl. Phys. Lett. 91 (2007) 031911.
[31] J. David, Y. Laurent, J. Lang, Structure de $MgSiN_2$ et $MgGeN_2$, Bull. Minér. 93 (1970) 153–159.
[32] D.C. Reynolds, D.C. Look, B. Jogai, C.W. Litton, G. Cantwell, W.C. Harsch, Valence-band ordering in ZnO, Phys. Rev. B 60 (1999) 2340–2344.
[33] J. Häusler, R. Niklaus, J. Minár, W. Schnick, Ammonothermal synthesis and optical properties of ternary nitride semiconductors Mg-IV-N_2, Mn-IV-N_2 and Li-IV_2-N_3 (IV = Si, Ge), Chem. Eur. J. 24 (2018) 1686–1693.
[34] L.C. Allen, Electronegativity is the average one-electron energy of the valence-shell electrons in ground-state free atoms, J. Am. Chem. Soc. 111 (1989) 9003–9014.
[35] J.B. Mann, T.L. Meek, L.C. Allen, Configuration energies of the main group elements, J. Am. Chem. Soc. 122 (2000) 2780–2783.